Thermal conductivity of multi-walled carbon nanotube sheets: radiation losses and quenching of phonon modes

2010 Nanotechnology 21 035709

(http://iopscience.iop.org/0957-4484/21/3/035709)

Nanotechnology **21** (2010) 035709 (11pp) doi:10.1088/0957-4484/21/3/035709

Thermal conductivity of multi-walled carbon nanotube sheets: radiation losses and quenching of phonon modes

Ali E Aliev[1], Marcio H Lima[1], Edward M Silverman[2] and Ray H Baughman[1]

[1] Alan G MacDiarmid NanoTech Institute, University of Texas at Dallas, Richardson, TX 75083, USA
[2] Northrop Grumman Space Technology, Redondo Beach, CA 90278, USA

E-mail: Ali.Aliev@utdallas.edu

Received 26 August 2009, in final form 11 November 2009
Published 7 December 2009
Online at stacks.iop.org/Nano/21/035709

Abstract

The extremely high thermal conductivity of individual carbon nanotubes, predicted theoretically and observed experimentally, has not yet been achieved for large nanotube assemblies. Resistances at tube–tube interconnections and tube–electrode interfaces have been considered the main obstacles for effective electronic and heat transport. Here we show that, even for infinitely long and perfect nanotubes with well-designed tube–electrode interfaces, excessive radial heat radiation from nanotube surfaces and quenching of phonon modes in large bundles are additional processes that substantially reduce thermal transport along nanotubes. Equivalent circuit simulations and an experimental self-heating 3ω technique were used to determine the peculiarities of anisotropic heat flow and thermal conductivity of single MWNTs, bundled MWNTs and aligned, free-standing MWNT sheets. The thermal conductivity of individual MWNTs grown by chemical vapor deposition and normalized to the density of graphite is much lower ($\kappa_{\mathrm{MWNT}} = 600 \pm 100$ W m^{-1} K^{-1}) than theoretically predicted. Coupling within MWNT bundles decreases this thermal conductivity to 150 W m^{-1} K^{-1}. Further decrease of the effective thermal conductivity in MWNT sheets to 50 W m^{-1} K^{-1} comes from tube–tube interconnections and sheet imperfections like dangling fiber ends, loops and misalignment of nanotubes. Optimal structures for enhancing thermal conductivity are discussed.

1. Introduction

Bulk samples of well-aligned carbon nanotubes exhibit fascinating behavior including highly anisotropic electrical and thermal transport properties. Theoretical predictions yield an extremely high thermal conductivity for individual single-wall carbon nanotubes (SWNTs), $\kappa = 6600$ W m^{-1} K^{-1} [1], and suggest their possible application for heat management systems [2]. For macroscopic devices, one must assemble a vast number of nanotubes in order to obtain a desired conductance. Then, interaction between confined nanotubes in bundles can partially decrease their rotational and vibrational freedom, lead to quenching of phonon modes and decrease the thermal conductivity.

On the other hand, for a long macroscopic device incorporating many tubes along the transport direction the tube ends provide a main obstacle for electron and heat transport. It is obvious to assume that bundling of long nanotubes into dense ropes can overcome this problem by providing additional bypass for effective transport. Below, by computer simulation, we show that, due to the high aspect ratio of CNTs, even weak van der Waals interactions between aligned nanotubes over long overlap distances (when the lateral overlap surface area is higher than the cross section of the carbon nanotube by a factor $\kappa_{\parallel}/\kappa_{\perp} = 342$) is sufficient to reduce the effects of thermal resistance at tube ends and tube–electrode interfaces.

We will restrict our discussion to the use of multi-walled carbon nanotubes (MWNTs) as a preferred choice for heat propagation: as the nanotube diameter increases, more optical phonon modes with longer mean free paths are excited at room temperatures. The higher strain fields in inner shells of MWNT can result in higher thermal conductivity

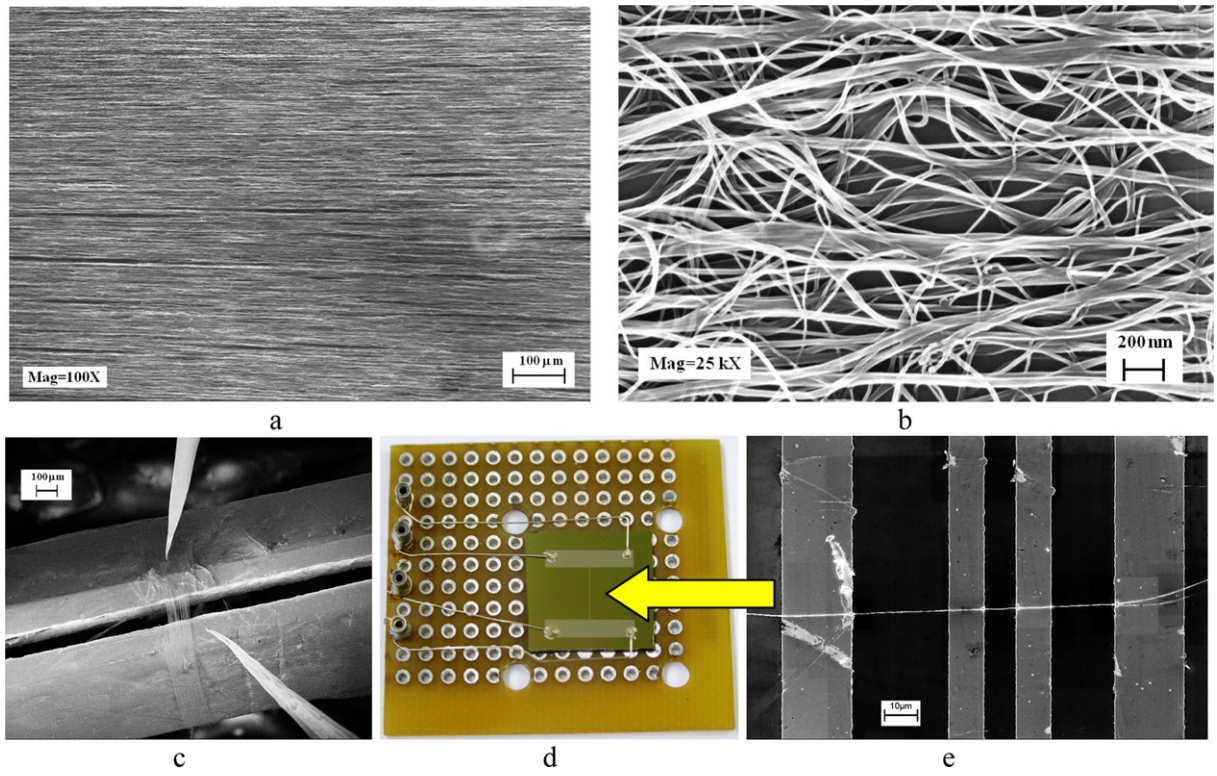

Figure 1. ((a), (b)). SEM images of a free-standing MWNT sheet at increasing magnification. (c) MWNT sheet attached to two bulk copper electrodes and fixed by the tungsten tips of a nanomanipulator. (d). Four-probe electrode cell, patterned by UV lithography on silicon substrate, attached to a circuit board. The layered conductive electrodes comprise three different metals: nickel–gold–titanium. (e). SEM image of four-probe electrodes (gray vertical electrodes are separated by dark trenches) with attached 100 nm diameter MWNT bundle.

compared to single-wall carbon nanotubes [3]. Moreover, it is natural to think that intrinsic defects (vacancies or conformations) should have much more severe effects in SWNTs (one-dimensional conductors) than in MWNTs (two-dimensional conductors). The neighboring shells in MWNTs provide effective additional channels for phonons to bypass the defective sites. Additionally, the outermost shell protects the inner shells from the environment.

Recently we have developed a new dry-state processing method for producing highly oriented, free-standing MWNT sheets that may become very attractive for thermal transport applications if challenges are overcome [4]. Higher alignment, a two-dimensional framework of MWNT sheets and extensive inter-tube overlap are potentially promising features for effective heat transport. However, the measurements of thermal conductivity versus electrode separation length and temperature show that heat transport in long free-standing samples is dominated by surface radiation, so that little heat energy is transferred by phonons for distances > 2 mm, which is attributed to the extremely low areal density of these sheets ($\sim$1 to $\sim$3 μg cm^{-2}) [5]. The thermal conductivity (κ) and thermal diffusivity (α) of highly aligned MWNT sheets (measured for short distances, $L < 2$ mm) are relatively low (50 ± 5 W m^{-1} K^{-1} and 45 ± 5 mm^2 s^{-1}, respectively) and mostly reduced by the low quality of CVD-grown carbon nanotubes (high numbers of structural defects), phonon scattering in bundles and imperfect alignment.

If extremely large surface area and high emissivity of carbon nanotubes cause the high surface radiation, then the solution is a dense bulk structure where the outermost nanotubes will screen radiation from the interior. However, coupling between nanotubes in bundles can suppress the phonon modes and decrease the transport abilities of individual MWNTs. The thermal conductivity (600 ± 100 W m^{-1} K^{-1}) of individual CVD-grown MWNTs (obtained by the 3ω method) is lower than theoretically predicted. Coupling within nanotube bundles and poor impedance matching at the tube–sink interface decreases the thermal conductivity down to 150 ± 20 W m^{-1} K^{-1}. A further decrease of effective thermal conductivity in MWNT sheets to 50 ± 5 W m^{-1} K^{-1} originates from tube–tube interconnections and sheet imperfections like fiber ends, loops and misalignment of tubes.

2. Experimental details

Highly oriented transparent nanotube sheets and yarns were drawn from the sidewall of a 300–350 μm tall MWNT forest, which was synthesized by a catalytic chemical vapor deposition method (CVD) [4]. Typical images of the suspended sheet taken by LEO 1530 VP scanning electron microscope (SEM) are shown at different magnifications in figures 1(a) and (b). The suspended sheet can be stored under tension between two parallel supporting rods, or directly

transferred to the two- or four-probe electrode assemblies shown below in figures 1(c)–(e).

To study the quenching of phonon modes, a four-probe electrode assembly was fabricated on non-doped, thermally oxidized silicon and glass substrates (10×10 mm^2) using UV lithography. Two sets of four-probe patterned substrates with different electrode separation were fabricated: 1 μm thick layered electrodes (nickel, 600 nm/gold, 300 nm/titanium, 100 nm) with electrode separations (from left to right in figure 1(e)) of 30, 10 and 20 μm, and the width of outer electrodes, 20 μm, and inner electrodes, 10 μm, respectively. The different inter-electrode separations enable our evolution of the contribution from tube/electrode interfaces. The top Ti layer provides satisfactory ohmic contact with the MWNTs.

A tiny MWNT ribbon drawn from the suspended sheet or MWNT forest and attached to the four-probe electrodes comprises large diameter (100–150 nm) bundles that are interwoven with small diameter bundles or single MWNTs. To choose a desired bundle or a single MWNT, we used a Zyvex nanomanipulator (Zyvex Inc., Nano-100A) equipped with four horizontal fingers that end in tungsten tips (chemically sharpened to 100 nm on the edge).

The quasi-2D structure of the MWNT sheet forms an almost perfect interface with the surface of smooth gold electrodes. However, the roughly round shape of large bundles prevents good electrical and thermal contact with the sink, since only a fraction of the exterior MWNTs in a bundle make contact. To minimize this problem, the large MWNT bundles were carefully flattened by a tungsten tip and squeezed into soft gold electrodes. Further improvement of the MWNT/electrode interface was obtained by deposition of platinum spots or an elongated strip using an FIB Nano200 (see figure 1(e)). However, it is worth noting here that long exposure to the high energy ion beam damages the MWNT structure.

Samples with small numbers of MWNTs in bundles have high resistance ($R > 0.5$ MΩ) and are very sensitive to the static potential, so they are difficult to handle. To test the quality of MWNT/electrode contacts, the resistances of the left (20 μm) and right (30 μm) end segments, compared with the resistance of the middle electrode separation (10 μm), were characterized by two- and four-probe methods using a Keithley 2425-C Source Meter and a low probe current, $I < 1$ μA.

Thermal characterization method. Thermal transport measurements were performed using the self-heating 3ω technique. The diffusive nature of MWNT electronic conductivity suggested the use of this technique for determining thermal transport along the one-dimensional (1D) conductor [5–7]. In this case, at low frequencies 1D heat flow can be expressed in terms of the third harmonic voltage signal $U_{3\omega}$ induced by an AC current $I_o \sin \omega t$ applied through the elongated sample (metallic wire, carbon fiber, nanotube or bundle, yarns or sheet). The AC current with frequency ω creates a temperature fluctuation in the specimen at double the driving frequency, 2ω. The interaction of the 2ω modulated resistance R with the 1ω current creates a third harmonic response on the electrodes used for potential measurements [7]:

$$U_{3\omega,\mathrm{rms}} = \frac{4I^3RR'}{\pi^4\kappa}\frac{L}{S}\frac{\mathrm{e}^{-\mathrm{i}(3\omega-\varphi)}}{\sqrt{1+(2\omega\gamma)^2}}, \tag{1}$$

where $I = U_I/(R + R_{\mathrm{ref}})$ is the applied AC current, R is the specimen resistance between the potential electrodes, R_{ref} is the series resistance in the balancing bridge, $R' = (\mathrm{d}R/\mathrm{d}T)$ is the temperature gradient of the resistance at the chosen temperature, L is the distance between potential electrodes, S is the cross-sectional area of the sample, κ is the thermal conductivity, $\gamma = L^2/\pi^2\alpha$ is the characteristic thermal time constant of the specimen for the axial thermal process and $\alpha = \kappa/\rho C_p$ is the thermal diffusivity. For comparison with bulk materials (graphite, copper, diamond) we normalize the measured thermal conductance to that for a hexagonally close-packed nanotube structure with a density of $\rho = 0.68\rho_{\mathrm{c}} = 1.54 \times 10^3$ kg m^{-3}, where $\rho_{\mathrm{c}} = 2.267 \times 10^3$ kg m^{-3} is the density of graphite and $C_p = 716$ J kg^{-1} K^{-1} is the heat capacity of graphite [8]. The diffusivity can be obtained from the frequency dependence of the phase lag of the third harmonic signal:

$$\tan\varphi \approx 2\omega\gamma = \frac{2\omega L^2}{\pi^2\alpha}, \tag{2}$$

or from the frequency dependence of the 3ω signal, $U_{3\omega}$, using equation (1). For thin, long samples in the low frequency limit one obtains the thermal conductivity:

$$\kappa = \frac{4I^3RR'}{\pi^4 U_{3\omega}}\frac{L}{S}. \tag{3}$$

All measurements were done under high vacuum ($P < 10^{-7}$ Torr) in a Janis Research VPF-475 cryostat to reduce radial heat losses through gas convection. To minimize static radial heat dissipation from samples we used a simple heat shield of aluminum foil. This measure reduced the apparent thermal conductivity of an MWNT sheet at 295 K by 10%. To reduce oxygen doping from ambient, each sample was kept in vacuum at 400 K for 48 h. This treatment significantly stabilized sample properties and increased measurement reproducibility.

For suspended MWNTs with low thermal coefficient of resistivity (TCR $\leqslant 7.6 \times 10^{-4}$ K^{-1}) and high resistance ($\sim 10^5$ Ω) the high $U_{1\omega}/U_{3\omega}$ ratio and the phase uncertainty of suspended shoulders suggested a nonconventional circuit for detecting the 3ω signal [7, 9]. Consequently, we designed a circuit configuration for two-probe measurements in which the $U_{1\omega}$ signal was compensated using a Wheatstone bridge. The Agilent 33220A Functional Generator, which has a spurious 3ω signal below 0.01 μV, was used in high impedance mode as a current source. The Stanford Research System SR830 DSP Lock-In Amplifier digitally detected the third harmonic signal (voltage amplitude and phase) across the sample, which contains valuable data for thermal transport analysis.

3. Simulation of heat distribution in single MWNT

To understand the peculiarities of heat transport in long MWNT bundles, let us estimate the heat distribution rate for individual MWNTs that are in bundles. When two parallel MWNTs overlap with each other at van der Waals contact distance, as shown in figure 2(a), heat from tube 1 first flows

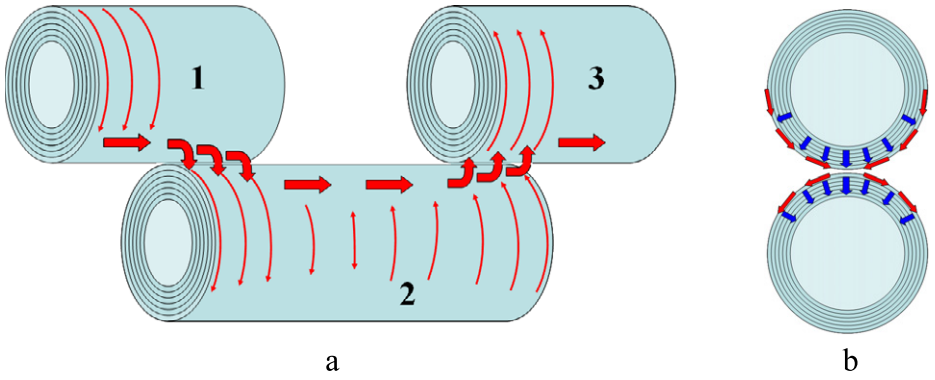

Figure 2. (a) Schematic representation of heat flow through tube–tube interface. Heat flows from MWNT #1 through MWNT #2 to MWNT #3. (b) Cross section of overlapping tubes.

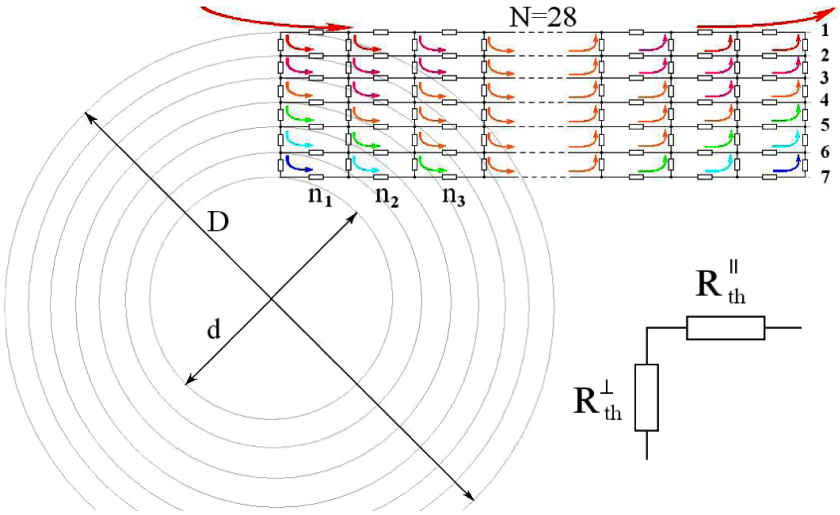

Figure 3. Schematic representation of MWNT intra-shell and inter-shell thermal resistances as an electrically equivalent circuit of resistors. Resistors $R_{\text{th}}^{\parallel}$ along the tube represent the thermal resistance of 100 nm long shell (10 nm on edges) with cross section of $0.34 \times P_i$ nm^2. Resistors $R_{\text{th}}^{\perp}$ connected perpendicular to the tube represent the thermal resistance between shells in the radial direction. The heat current is shown by colored arrows (the blue colored arrows correspond to the lowest heat flow and red arrows to the highest one).

through the outermost shell of tube 2 and then successively penetrates into progressively deeper inner shells of tube 2.

This simple intuitive picture of MWNT interconnection implies that the conducting path will strongly depend upon the anisotropy factor, $\xi = \kappa_{\parallel}/\kappa_{\perp}$. Graphite (pyrolytic form) has the highest anisotropy of thermal conductivity among all natural materials, $\xi_{300\text{ K}} = 342$ [8]. Despite similarities of heat flow mechanisms in graphite and MWNTs, a high density hexagonally packed MWNT structure (like an idealized bundle of equal-diameter MWNTs) must have a much lower anisotropy of thermal and electrical conductivities—due to a contribution of the circumferential bypass pathway to perpendicular conductivity. As soon as the heat is introduced into the outer shell of MWNT #2 the high thermal conductivity along the graphene layer transfers heat at a high flow rate in the circumferential direction, as well as along the tube.

Let us assume we introduced the heat current from the left edge of the outermost shell of MWNT #2 of figure 2(a) (red arrow in figure 3) having 10 nm diameter and comprising seven shells. For simulation of the heat distribution along and perpendicular to the tube we employed the equivalent circuit representation for the MWNT shown in figure 3 which ignores the possible diameter dependence of per area thermal resistance for thermal transport within and between wall layers. In the first approximation, the equivalent circuit of the MWNT structure could be depicted by a series of elements $R_{\text{th}}^{\parallel}$ aligned along the cylindrical graphene sheets of individual walls and elements $R_{\text{th}}^{\perp}$ aligned perpendicular to these walls and tied together as nodes as shown in figure 3. Simulation of the current flow through each resistive element and corresponding potential drops were evaluated using the commercial software package, Circuit Maker 2000 (ACCEL Tech. Inc., USA).

Taking into account the van der Waals spacing between shells ($h = 0.34$ nm), the diameter of the innermost shell is $d = 5.92$ nm. The cross-sectional surface area of each shell S_i, the circumferential length of shells P_i, the thermal conductance

Table 1. Geometrical and thermal parameters used for simulation of heat current distribution in 1 μm long, 10 nm in diameter MWNT comprising seven shells. (Note: last row shows the sum of column, unless marked (*), when it shows the averaged value.)

#	S (nm^2)	P (nm)	$\Lambda^{\parallel} \times 10^{9}$ (W K^{-1})	$R^{\parallel}_{\rm th} \times 10^{-6}$ (W^{-1} K)	$\Lambda^{\perp} \times 10^{6}$ (W K^{-1})	$R^{\perp}_{\rm th} \times 10^{-3}$ (W^{-1} K)
1	10.32	31.4	6.2	161	161	6.2
2	9.6	29.3	5.76	174	150	6.66
3	8.86	27.1	5.3	188.7	139	7.2
4	8.14	25	4.88	205	128	7.8
5	7.4	22.9	4.44	225	118	8.5
6	6.69	20.7	4	250	107	9.3
7	5.95	18.6	3.57	280	96	10.4
Σ	56.8	25*	34.15	205*	21.4	56.1

along, $\Lambda^{\parallel}_i$, and perpendicular to shells, $\Lambda^{\perp}_i$, and corresponding thermal resistances $R^{\parallel}_{\rm th}$ and $R^{\perp}_{\rm th}$, for a 1 μm long tube are shown in table 1.

The continuously distributed intra-shell thermal resistance of a 1 μm long tube in our simulation was first represented by 10 discrete resistors with nominal resistance $R^{\parallel}_{\rm th}/10$, respectively. This resistance increases toward the innermost layers due to the decrease of the cross-sectional area of shells (see table 1). The inter-shell resistance between shells can also be depicted as 11 parallel resistors, $R^{\perp}_{\rm th} \times 10$, as shown in figure 3. Each cell in figure 3, shown as n_i, represents a 100 nm long segment of MWNT. The simulated current distribution is very sensitive to the discretization on the edge cells. To improve the current convergence the edge cells n_1 and n_{10} were again split into 10 cells with resistor values $R^{\parallel}_{\rm th}/100$ and $R^{\perp}_{\rm th} \times 100$, respectively. Then the total number of cells for simulation was $N = 28$.

Simulation of heat current demonstrates (figure 4) that heat introduced to the outer shell is evenly distributed (on a per shell cross-sectional area basis) to all shells within a short distance, $L \sim 50$ nm (see the inset to figure 4). At the left edge ($L < 10$ nm) the heat flows mostly in the outer shell. The relatively high in-plane resistance of a cylindrical shell turns the heat current down to the next shell, so that within 50 nm the heat current density is uniformly distributed along all shells. Naturally, the total heat current flowing through the outer shell is always higher than the current in the next shell due to the higher cross-sectional area (see table 1). It is easy to observe that heat current equilibration is a function of anisotropy factor ξ and number of shells, but independent of the absolute value of thermal conductivity, κ. The obtained results suggest an optimal size for a sputtered metallic spot for enhancing the thermal contact.

4. Thermal resistance of tube–tube coupling

Tube–tube interaction in MWNTs are primarily caused by van der Waals forces, except for special situations when local charge or covalently bonded functional groups introduce additional electrostatic fields. The heat transfer rate between non-parallel nanotubes is extremely low because the van der Waals forces interact at short distances, $U \sim -1/r^6$, and the cylindrical shape of MWNTs severely limits the interaction

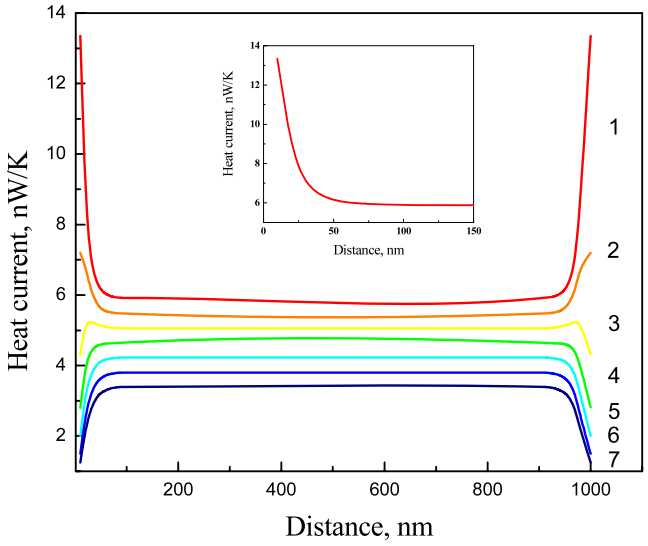

Figure 4. Distribution of the heat current along MWNT #2 comprising seven shells. The outer shell current corresponds to curve 1 (red). The inset shows the extended curve 1 at the left edge.

surface area. Despite this limitation, a long interaction distance, such as between bundled nanotubes, can overcome this problem. What overlap length is needed to effectively eliminate the effect of thermal resistance between coupled nanotubes? Taking into account the weak van der Waals interaction between nanotubes and tube surface curvature, we can estimate the effective overlap length that is needed to provide the same surface area as the cross section of a given MWNT with average diameter of 10 nm. Then we can multiply the obtained length by a factor $\xi = 342$, which is the ratio of basal plane conductivity to the perpendicular one for graphite, to obtain an estimate of the needed overlap length between nanotubes.

Here we consider only van der Waals coupling between the perfect tubes with intrinsic thermal conductivity between shells of $\kappa_{\perp} = 1.75$ W m^{-1} K^{-1} and ignore any additional interfacial Kapitza resistances [10, 11]. The Kapitza resistance provides a barrier to heat flow that is associated with differences in the phonon spectra of two phases and possible weak contact at the interface. Despite the random chirality of shells in interacting tubes, the phonon spectra of tubes having about the same diameter could be very similar. However, a serious practical problem might be that the thermal conductivity of the outermost shell might be much lower than expected, possibly because of a residual surface carbon, bounded oxygen and structural defects. The effect of intrinsic defects have been approximated by reducing $\kappa^{\perp}$ from 5.7 W m^{-1} K^{-1} in graphite to 1.75 W m^{-1} K^{-1} for MWNTs (using the thermal conductivity of an individual MWNT of 600 W m^{-1} K^{-1}, from this work and $\xi = 342$, the ratio for graphite).

The interaction surface area between two parallel identical tubes can be simply estimated as $A = \sigma L$, where σ is an effectively interacting segment of the nanotube circumference and L is the overlap length. The van der Waals attraction energy decays fast with increasing nanotube separation (to one-

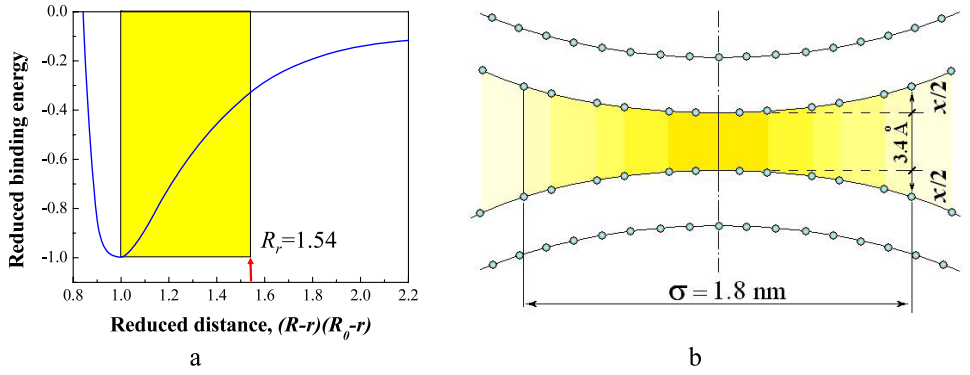

Figure 5. (a). The universal potential for graphitic structures [13]. Surface area under the curve determines the normalized tube separation, $R_r = 1.54$. (b). Cross section of two superimposed MWNT. Separation between outermost shells x is increased when moving apart from the axis line between tube centers.

half for 1 Å from equilibrium, 3.4 Å, and almost vanishes at 4–5 Å) [12].

Using the Lennard-Jones potential for interaction of two atoms at a distance x:

$$u(x) = -\frac{A}{x^6} + \frac{B}{x^{12}}, \tag{4}$$

where A and B are the attractive and repulsive constants, and the continuum model for the binding energy between two identical, parallel tubes in [13] was found to be the universal potential for graphitic structures, which can be applied to estimate the effectively interacting segment. The numerical integration of the surface area under an attractive potential curve above the reduced equilibrium distance ($R_r = (R - r)/(R_o - r) = 1$, [13]) gives us the normalized tube separation, $R_r = 1.54$ (figure 5(a)), which corresponds to $(R - r) = 5.236$ Å. Obviously, this distance is much smaller than the cutoff distance $r_{\text{cut}} = 8.875$ Å found in [14] or $r_{\text{cut}} = 7.32$ Å for single-walled carbon nanotubes in [15]. For an MWNT with an outermost shell diameter of 10 nm (the sum of the radii of the interacting objects r =10 nm) this gives an effective separation $\Delta x_{\text{eff}} = (R - r) - 3.4$ Å $= 1.84$ Å. Hence, the increase of separation from equilibrium to $\Delta x/2 = 0.92$ Å corresponds to the effective interaction segment of $\sigma = 1.8$ nm (see figure 5(b)). Though we can say that on the width of the interacting segment of 1.8 nm, the binding energy is the same as for a van der Waals separation distance of 0.34 nm. Then, the tube–tube interacting surface area we need to minimize the interfacial thermal resistance is: $L = S_\Sigma \xi/\sigma = 31.5$ μm, where $S_\Sigma = 56.8$ nm^2 is the cross-sectional surface area of the tube (see table 1).

We can here neglect heat resistance to the next shells because these shells have a 17.4 times larger interacting surface area (the circumference length, $P_1 = 31.4$ nm) and the above computer simulation shows very fast redistribution of heat current flow within $L < 50$ nm. The obtained tube–tube overlap length is valid for nanotubes suspended in air or vacuum ($\varepsilon \sim 1$). For an MWNT/sink interface reinforced with deposited metal the heat transfer can be 17.4 times higher, since now the whole circumferential surface participates in the heat exchange. Therefore, 2–5 μm long metallic pads deposited on MWNT bundles are quite sufficient for high quality sink terminals.

5. Results and discussion

5.1. Black-body radiation from an MWNT sheet

Measurement of apparent κ for a free-standing MWNT sheet as a function of electrode separation using the 3ω method revealed a quadratic decrease of the third harmonic signal and consequently an increase in the derived κ for longer samples (figure 6(a)). Below 2 mm sample length, the apparent κ saturates at 50 ± 5 W m^{-1} K^{-1}, which will be shown to correspond to the real thermal conductivity.

The question is, what causes an increase of apparent κ with the increased length of the sheet studied? For an MWNT sheet with extremely large surface area the apparent κ can be higher than the actual value, $\kappa_{\text{ap}} = \kappa + \kappa_{\text{loss}}$, due to radial heat loss through radiation [7]:

$$\kappa_{\text{loss}} = \frac{16\varepsilon\sigma T_o^3 L^2}{\pi^2 d}, \tag{5}$$

where $\sigma = 5.67 \times 10^{-8}$ W m^{-2} K^{-4} is the Stefan–Boltzmann constant, ε is the emissivity, d is the average diameter of individual 1D heat channels and $T_o = 295$ K is the environmental temperature. For porous carbon materials we can use the black-body emissivity of $\varepsilon = 1$. The solid line in figure 6(a), plotted using equation (5), dependence of κ_{loss} on L, shows a reasonably good agreement with the measurement. The fitting parameters, shown in the insets, yield the diameter $d = 140$ nm of a cylindrical rod that determined the radiation surface area of the MWNT sheet. This value is surprisingly close to the bundle diameter ($d = 130 \pm 20$ nm) that we found from atomic force microscopy measurements [5].

Our hypothesis, that the apparent thermal conductivity is increased by radiative heat loss, was tested by comparing the temperature dependence of κ for long and short samples. At low temperatures the black-body radiation should be significantly reduced and one can measure the intrinsic phonon transport parameters. Figure 6(b) shows that the determined κ for all samples are comparable below $T = 150$ K. Above 150 K, the measured κ of long samples (7.6 and 5.4 mm) are substantially higher than that of the shortest sample ($L = 0.37$ mm) studied here. It is worth noting that for all the above experiments the temperature modulation of the suspended part

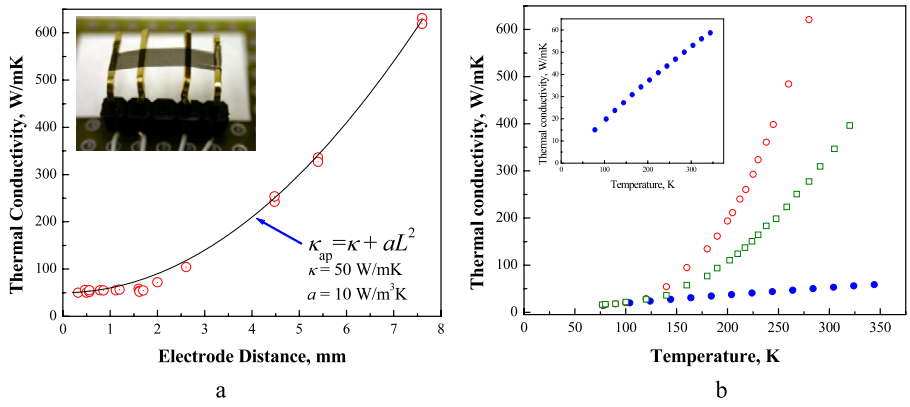

Figure 6. (a) Dependence of apparent κ (open circles) on inter-electrode separation (L) for an MWNT sheet measured using the 3ω method. The solid line is a data fit that uses the quadratic dependence of κ_{loss} on L from equation (5). The fitting parameters are shown in the right bottom inset. The top inset shows a four-probe cell attached to a nanotube sheet for these measurements. (b) The temperature dependence of apparent κ for three different lengths: 7.6 mm (red open circles), 5.4 mm (green open squares) and 0.37 mm (blue solid circles). The inset provides an expanded plot for the $L = 0.37$ mm sample.

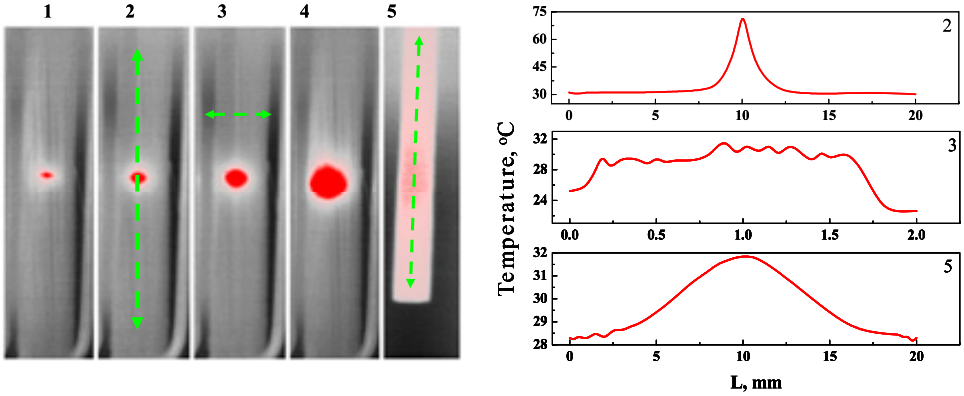

Figure 7. Distribution of thermal spots along the MWNT sheet (20 layers) excited by red laser (830 nm) and measured using an infrared camera. The power of the excitation beam increases from left to right in the picture columns (10, 20, 30 and 50 mW for pictures 1–4, respectively). For comparison, the picture in column 5 shows the temperature distribution in a Ge strip excited with power 80 mW. The temperature distribution along the green arrows on the left is shown in temperature plots on the right.

Table 2. Thermal and electrical transport parameters of MWNT sheet.

Sample	Thermal conductivity (W m^{-1} K^{-1})	Thermal diffusivity (mm^2 s^{-1})	Sheet resistance ($\Omega/\square$)
MWNT sheet, $\parallel$	50	45	500
MWNT sheet, $\perp$	2.1	8.2	30 000

of the sample did not exceed 5 K. Therefore, we believe that for MWNT sheets drawn from 300 μm high forest radiation losses dominate at room temperature for sheet lengths above 2 mm. The radial heat current was an order of magnitude higher than the axial current for a sheet length of ~7.6 mm. Table 2 summarizes the obtained transport parameters along and perpendicular to the nanotube alignment in the MWNT sheets.

The temperature distribution along the MWNT sheets (observed using a MobIR M4 thermal camera, Wuhan Infrared Tech. Co.) confirms the high radiation loss from the surface. The heat spot created by an IR laser (830 nm) is localized around the excited beam and expanded only to 1–2 mm along the sheet, whereas for a Ge strip of 0.5 × 2 × 20 mm^3 (right column in figure 7) with almost the same κ (58 W m^{-1} K^{-1}) the temperature distribution is much more uniform. Due to the high reflectivity of the Ge strip the incident beam power was increased to 80 mW. Green arrows in the left columns 2, 3 and 5 mark the line used for measurement of the temperature profile shown on the right. The white elongated lines radiating from the red laser spot are heat conduction channels arising from dense clusters of large diameter MWNT bundles. Despite high radiation from the more homogeneously distributed MWNTs in other regions of the sheet, the large bundles conduct thermal energy over long distances. Diagram 3 shows the temperature profile across the sheet taken 5 mm above from the laser spot. The outer layer of nanotubes in a bundle shield the black-body radiation from the inner part and thereby provides the long-range heat channel. However, bundling of individual tubes should quench some phonon modes that contribute to the thermal conductivity and provide additional phonon scattering.

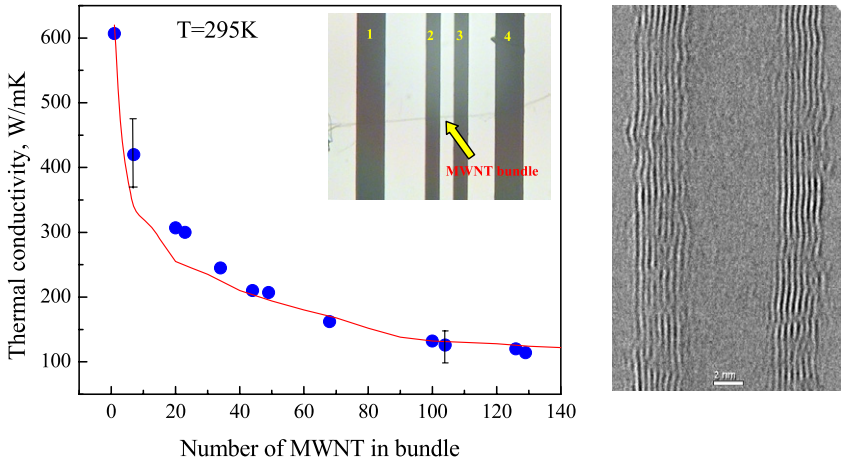

Figure 8. The thermal conductivity of MWNTs measured by the 3ω method at room temperature as a function of the number of tubes in a bundle. The solid line is a fitting curve following equation (7). The inset shows an SEM image of four-probe gold patterned substrate with attached MWNT bundle. Right inset: TEM image of ∼10 nm MWNT comprising 7–8 shells.

Below we experimentally study phonon scattering in bundles having different numbers of tubes in a bundle.

5.2. Phonon scattering in bundles

Figure 8 shows that tube–tube coupling decreases the room temperature thermal conductivity of MWNT bundles by a factor of four relative to that for a single tube. The thermal conductivity of a single MWNT measured for 10 μm electrode separation and normalized to the ideal high density structure (the inner void space was subtracted) with van der Waals spacing between shells is 600 ± 100 W m^{-1} K^{-1}. This value is much lower than theoretically predicted κ = 6600 W m^{-1} K^{-1} [1] and that experimentally confirmed for individual nanotubes [6], κ = 3000 W m^{-1} K^{-1}. It is well known that MWNTs grown by CVD are more defective than those grown by arc-discharge or laser-ablation methods [16]. The coupling in nanotube bundles exponentially decreases the thermal conductivity. The decrease of κ with increasing bundling saturates at 150 ± 15 W m^{-1} K^{-1} when the diameter of MWNT bundles reaches 120–150 nm. The obtained κ of those bundles is consistent with the thermal conductivity of an MWNT sheet in which nanotubes in well-aligned bundles (with average diameter 140 nm [5]) are interwoven with poorly oriented nanotubes that laterally interconnect these bundles (see figure 1(b)).

The electrical resistance of a single MWNT (D = 10 nm, d = 5 nm) measured by the four-probe method was 56 ± 5 kΩ per 1 μm length (further denoted as kΩ/μm). This resistance agrees with data of other authors presented in table 3. The obtained value was used as a reference for further measurements and for rough estimation of the number of individual tubes in bundles. For each sample the resistance of the central section on the four-electrode substrate (electrodes 2–3 in the inset to figure 8) was first measured. Then the resistances of the left and right segments (with electrode separation 20 and 30 μm) were compared with the first one. If the normalized resistance was within 10% of the reference, we proceeded with thermal measurements on the sample.

Table 3. Electrical resistance of single MWNTs grown by different methods. CVD—chemical vapor deposition, AD—arc-discharge methods. T = 295 K.

Growth method	R (kΩ)	L (μm)	R (kΩ μm^{-1})
CVD$_{\text{current work}}$	560	10	56
AD [17]	28	0.8	35
CVD1 [18]	230	5.3	43
CVD2 [18]	23	0.3	76.7
CVD3 [18]	50	0.5	100
AD [19]	6	0.4	15
Graphite	$\rho = 7.84 \times 10^{-6}$	—	54.9[a]

[a] The resistance of graphite strip with the same cross section as a 10 nm MWNT.

The low frequency dispersion band diagram $\omega(k)$ of an MWNT is similar to that of graphite and has four acoustic branches, which originate from the Γ point of the Brillouin zone with zero frequency ω at zero wavevector, k (see figure 9). In order of increasing frequency ω these are doubly degenerated transverse (shear) modes involving out-of-plane motion (TA), in-plane 'twist' modes (bond bending, TW) and in-plane longitudinal modes (bond stretching, LA). The TW and LA modes involve only movement of atoms tangential to the tube surface and thus are expected to couple very weakly to other tubes in a bundle. However, in tight bundles at low wavevectors the TW mode becomes an optical mode because of the presence of a nonzero shear modulus between neighboring tubes [20]. Simple estimation of the contribution from only acoustical modes (am-LA, TW, 2TA) to the thermal conductivity using constant inelastic phonon relaxation time τ [20]:

$$\kappa_{zz} = \sum C \overline{V}_z^2 \tau, \tag{6}$$

where C = 700 J kg^{-1} K^{-1}, $\upsilon_z = (1/4\sum \overline{V}_{am}^{-3})^{-1/3}$ and $\tau \sim 4.6$ ps are the specific heat, group velocity and relaxation time of a given phonon state, shows that even total quenching of the lowest acoustical phonon modes (two TA and one TW) only reduces κ by 28.5%. In fact, at room temperature there are over 15 activated optical modes in MWNTs that can contribute

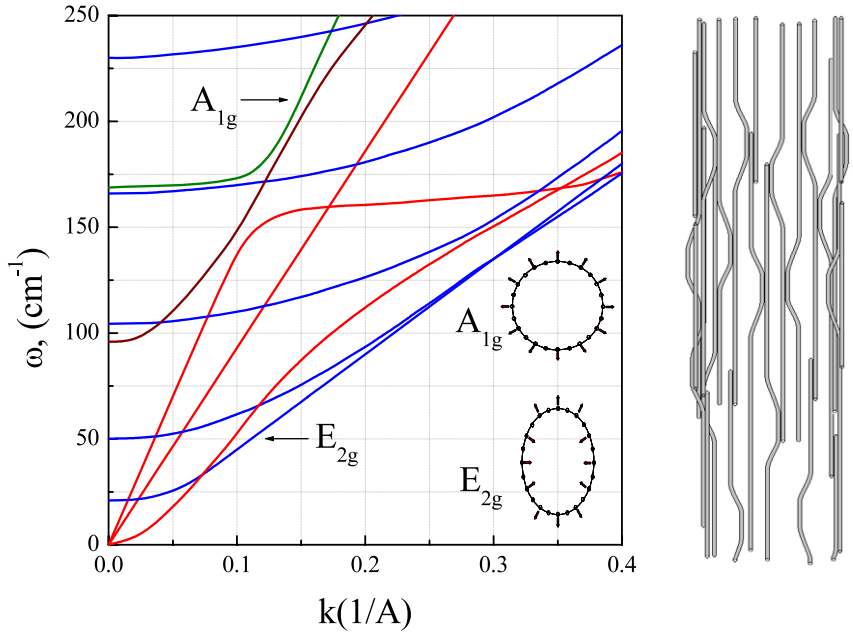

Figure 9. Low energy phonon dispersion relations for an isolated (10, 10) nanotube [20]. There are four acoustic modes (red lines): two degenerate TA modes ($v = 9$ km s^{-1}), a 'twist' mode ($v = 15$ km s^{-1}) and one LA mode ($v = 24$ km s^{-1}). Right insert: schematic view of an optimal structure for an MWNT assembly for heat management, which preserves the vibrational freedom of individual nanotubes and shields against heat radiation by using a dense outermost MWNT layer.

to κ. Two of these low-lying branches are particularly significant, the lowest nonzero optical branch corresponding to the squeezing modes associated with a change of the circular tube cross section to elliptical, E_{2g}, and a radial breathing mode, A_{1g}. These low-lying optical phonon modes have group velocities and frequencies comparable to the acoustic modes, and at high temperatures their contribution to the phonon mean free path is dominant. Since these modes involve out-of-plane motion, they are substantially suppressed in bundles. This phenomenon is widely used for identification of SWNT bundling using Raman scattering spectra. Note also that in MWNTs the A_{1g} and E_{2g} are shifted towards lower frequencies as $\omega(D) = 234/D$ nm and $\omega(D) = (6.28/D)^2$, respectively, and buried in the shoulders of excitation light in Raman spectra.

Berber *et al* mention [1] that strong tube–tube coupling can decrease the high temperature κ of SWNT bundles by an order of magnitude relative to isolated tubes. The same occurs for graphene layers when they are stacked in graphite—interlayer interactions quench the thermal conductivity of this system by nearly an order of magnitude. Moreover, for large diameter nanotubes ($D > 2$ nm), especially those with few walls, van der Waals forces between adjacent nanotubes can substantially deform them, destroying cylindrical symmetry [21]. The experimentally observed flattering of the tubes along the contact region in MWNTs [22] can reinforce tube–tube coupling and cause additional suppression of TW and low-lying optical phonon modes. Also, strong coupling in dense bundles restores the conditions for intensive umklapp (three-phonon process) processes [23] which were substantially suppressed in one-dimensional systems.

To take into account the above-mentioned mechanism that reduces thermal conductivity, we can assume that each additional nanotube in the bundle increases the average number of adjacent interconnections to $2n/N$, where n is the total number of connections in the bundle and N is the number of tubes. (For an infinite number of equal-diameter tubes in a bundle $2n/N \to 6$, i.e. each tube is surrounded by six parallel adjacent tubes.) We can fit the experimental data in figure 8 by using the equation

$$\kappa = 600 - 80\left(\frac{2n}{N}\right), \tag{7}$$

which shows that each adjacent interconnection decreases the normalized thermal conductivity by approximately 80 W m^{-1} K^{-1}. The obtained fitting curve is not smooth since the addition of each new nanotube to a bundle contributes a geometrically determined weight that is not a continuous function of N. The bend of the fitting curve takes place at some 'magic' numbers $N = 1, 7, 19, 37, 61, \ldots$, which might not be experimentally observed even for MWNTs having equal diameters, because of imperfect nanotube packing in bundles.

Let us suppose that we have achieved a 1 m long freely suspended carbon nanotube with $\kappa = 3000$ W m^{-1} K^{-1}. Radial radiation from the surface will dissipate four orders of magnitude higher heat energy ($\kappa_{\text{loss}} = 2.45 \times 10^8$ W m^{-1} K^{-1} for a 10 nm diameter nanotube) than the heat that propagates along the tube. For a 1 cm long MWNT the radial losses are still one order of magnitude higher than the axial thermal conductivity. Both radiation and thermal conductivity equally contribute to heat dissipation from a hot side that is 3.5 mm distant.

A key question is 'What is the optimal structure of a nanotube assembly to obtain the highest thermal conductivity for a long heat management system?' As we have seen above, to reduce the radial radiative heat loss from the surface of MWNTs we need to assemble the nanotubes in a dense structure where an outer shell prevents radiation from the interior (or we need to make a thick structure that achieves the same goal of providing mostly nanotubes whose heat radiation is shielded). However, to reduce inter-tube scattering and dampening of thermal vibrations in bundles the tubes should touch each other only over short distances, while still providing sufficient overlap to transfer thermal energy between nanotubes. Taking into account the strong van der Waals interaction between nanotubes, we estimated above the optimal overlap length to be $L \sim 30$–35 μm. Now, if we want to preserve the high individual nanotube κ (at least $\kappa > 400$ W m^{-1} K^{-1}, better than in copper and much better on a gravimetric basis) the nanotubes should touch each other over less than 2–3% of their total length, which provides a total MWNT length of 1.2–1.8 mm (assuming the same quality of nanotubes as presently investigated). A schematic sketch of the preferable structure of a 3D MWNT cable with short overlap in inner tubes is shown in figure 9 (right picture).

6. Conclusions

The thermal conductivity of single MWNTs measured for 10 μm electrode separation and normalized to the highest possible density structure (with subtracted inner void space) was 600±100 W m^{-1} K^{-1}. The low structural quality of CVD-grown MWNTs, compared to arc-discharge- or laser-ablation-produced MWNTs, can explain the obtained low thermal conductivity. We have experimentally demonstrated that bundling decreases the thermal conductivity by about a factor of four (150±15 W m^{-1} K^{-1}). Quenching of phonon modes in bundles, reinforced by radial deformation of carbon nanotubes by van der Waals forces, substantially reduces the transport abilities inherent for individual carbon nanotubes. Very recent experimental observation of the thermal conductivity decrease in few-layer graphene flakes (the thermal conductivity reduces with the increasing number of layers for $n = 2$, 3, and 4 atomic layers) [24, 25] is apparently caused by the same mechanism as quenching of phonon modes in carbon nanotubes.

We believe the MWNT structures are a better choice for phonon propagation in heat management systems than SWNTs: as the nanotube diameter increases, more optical phonon modes are excited which contribute to the heat flow. Moreover, it is natural to think that intrinsic defects produce much more severe effects in SWNTs than in MWNTs. The neighboring shells in MWNTs provide effective additional channels for phonons to bypass the defective sites. Additionally, the outermost shell protects the inner shells from the environment.

The extremely high surface area of MWNT sheets and ideal black-body emissivity cause heat radiation even for very low temperature gradients. To avoid heat dissipation in large thermal management systems, we propose bulk MWNT structures with a dense outer layer preventing radiation from lower density inner regions parts (figure 9, right). Computer simulation of individual MWNTs shows that heat applied to the outermost shell of a single MWNT is distributed among the shells within about 50 nm. However, heat transfer between tubes by sidewall interaction is a relatively weak process because of the small connecting surface areas of cylindrical tubes and the low phonon transport for non-covalent directions. A 30 μm tube–tube overlap length is required for a 10 nm in diameter MWNT to avoid a thermal impedance increase due to a tube end. To achieve high thermal conductivity in long MWNT cables (at least $\kappa > 400$ W m^{-1} K^{-1}, higher than for copper) the nanotubes should touch each other over less than 2–3% of their total length, which provides a total MWNT length of 1.2–1.8 mm.

Work on providing high thermal conductivity for long cables should focus on improving the quality of individual tubes, which can give an additional factor of five (600 → 3000 W m^{-1} K^{-1}) in thermal conductivity enhancement. This is a very challenging task because the current trend shows that attempts to grow a taller spinnable forest for sheet and yarn fabrication decreases the quality of CVD-grown MWNTs.

Acknowledgments

We thank M Zhang and S Fang for providing the MWNT sheets and G K Hemani for four-probe substrates. This research was supported by the Strategic Partnership for Research in Nanotechnology (SPRING) via the AFOSR, NSF NIRT grant DMI-0609115 and a Northrop Grumman Space Technology grant, and Robert A Welch Foundation grant AT-0029.

References

[1] Berber S, Kwon Y-K and Tomanek D 2000 *Phys. Rev. Lett.* **84** 4613–6
[2] Ajayan P M and Zhou O Z 2001 *Carbon Nanotubes* (*Topics Applied Physics* 80) ed M S Dresselhaus, G Dresselhaus and Ph Avouris (Berlin: Springer) chapter (Application of Carbon Nanotubes) pp 391–425
[3] Kim T, Osman M A, Richards C D, Bahr D F and Richard R F 2007 *Phys. Rev.* B **76** 155424
[4] Zhang M, Fang S, Zakhidov A A, Lee S B, Aliev A E, Williams C D, Atkinson K R and Baughman R H 2005 *Science* **309** 1215–9
[5] Aliev A E, Guthy C, Zhang M, Fang S, Zakhidov A A, Fischer J E and Baughman R H 2007 *Carbon* **45** 2880–8
[6] Kim P, Shi L, Majumdar A and McEuen P L 2002 *Physica* B **323** 67–70
[7] Lu L, Yi W and Zhang D L 2001 *Rev. Sci. Instrum.* **72** 2996–3003
[8] Lide B R (ed) 2001 *CRC Handbook of Chemistry and Physics* 82nd edn (New York: CRC Press) pp 12–221
[9] Choi T Y, Poulikakos D, Tharian J and Sennhauser U 2005 *Appl. Phys. Lett.* **87** 013108
[10] Kapitza P L 1941 *Zh. Eksp. Teor. Fiz.* **11** 1
Kapitza P L 1941 *Sov. J. Phys.—JETP* **4** 121 (Engl. Transl.)
[11] Swartz E T and Pohl R O 1989 *Rev. Mod. Phys.* **61** 605–68
[12] Yakobson B I and Couchman L S 2006 *J. Nanoparticle Res.* **8** 105–10
[13] Girifalco L A, Hodak M and Lee R S 2000 *Phys. Rev.* B **62** 19 13104–10
[14] Wei C, Cho K and Srivastava D 2003 *Appl. Phys. Lett.* **82** 2512

[15] Brenner D W, Robertson D H, Elert M L and White C T 1993 *Phys. Rev. Lett.* **70** 2174
[16] Salvetat J-P *et al* 1999 *Adv. Mater.* **11** 161–5
[17] Langer L *et al* 1996 *Phys. Rev. Lett.* **76** 479–82
[18] Ahlskog M *et al* 2001 *J. Low Temp. Phys.* **124** 335–52
[19] Stojetz B *et al* 2004 *New J. Phys.* **6** 27
[20] Popov V N, Van Doren V E and Balkanski M 2000 *Phys. Rev.* B **61** 3078–84
[21] Ruoff R S, Tersoff J, Lorents D C, Subramoney S and Chan B 1993 *Nature* **364** 514–6
[22] Avouris Ph *et al* 1999 *Appl. Surf. Sci.* **141** 201–9
[23] Cao J X 2004 *Phys. Rev.* B **69** 073407
[24] Balandin A A *et al* 2008 *Nano Lett.* **8** 902–7
[25] Ghosh S *et al* 2009 *Proc. MRS-2009 Spring Mtg (San-Francisco)*